Proterozoic crustal imbrication imaged beneath the Cheyenne belt in southeast Wyoming from the Laramie array teleseismic data

Steven Hansen and Ken Dueker
University of Wyoming, Dept. of Geology and Geophysics, Laramie, Wyoming

Abstract-

High resolution teleseismic results are presented from the Laramie array revealing strong evidence for crustal imbrication across the Cheyenne belt in southeast Wyoming (Fig. 1). This conclusion is derived from P and S wave receiver function images as well as a teleseismic P wave tomography model. One difficulty in this area is the presence of the Laramie Basin which introduces high amplitude free-surface reverberations into the P wave receiver function. To aid in interpretation of the P wave results, S wave receiver functions are also calculated in this study. The S wave dataset has lower fold and resolution but has proven useful for validating the P wave results due to the lack of interfering basin reverberations. To calculate the receiver functions, we extend the deconvolution methodology of Bostock (2004) to S wave data and develop a method of source function spectrum estimation which exploits the inherent spectral differences between the earthquake source functions and the receiver functions. Source function estimation is accomplished by smoothing the observed P wave log-spectra via a least-squared fit spline function.

Both P and S wave receiver function images (Fig. 2 and 3) find a "double-Moho" structure north of the Cheyenne belt which is interpreted to be the manifestation of underthrust Proterozoic lower crust. The Archean Moho is imaged at 41–43 km depth terminating laterally near the inferred surface location of the Cheyenne belt. A deeper velocity step is found at 60–62 km depth and appears to be laterally contiguous with the Proterozoic Moho of the northern Colorado Province. Modeling of P and S wave receiver function amplitudes suggests a 6.4 to 7.4 km/s velocity step across the Archean Moho and a 7.4 to 7.9 km/s velocity step across the deeper imbricated Proterozoic Moho. It is thought that the block directly south of the Cheyenne belt is an accreted arc terrane and we speculate that the observed 7.4 km/s layer is the imbricated arc lower crust. South of the Cheyenne belt, the P wave receiver function image finds the Proterozoic Moho dipping ~7° northwest consistent with observed backazimuth dependent Pms amplitudes.

The P wave tomography model (Fig. 4) shows a 14% lateral P wave velocity contrast in the upper 15 km of crust across the Cheyenne belt. This velocity contrast can be explained as a combination of the northwest thickening of the Laramie basin and by the ~0.5 km/s velocity contrast in the upper-crust across the Cheyenne belt found by the refraction study of Gohl and Smithson (1994). In addition, south of the Cheyenne belt, a low velocity body is found in the mid to lower crust which dips to the north and extends to a depth of 61 km beneath the Cheyenne belt. We interpret this body as underthrust Proterozoic lower crust (Fig. 5), which is consistent with our receiver function findings. Based on the deformation history of the Laramie Mountains, we speculate that imbrication of the Proterozoic lower crust was contemporaneous with the 1.76 Ga uplift and deformation of the 50-km-wide Palmer Canyon block immediately north of the Cheyenne belt and thus, the Cheyenne belt has retained crustal structure associated with the Proterozoic accretion of the Colorado Province.

Figure 1. a) Topography, stations, and crustal shear zones. Geographic features denoted as: SM, Sierra Madres; MB, Medicine Bow Mountains; LM, Laramie Mountains. In the Laramie Mountains, the Palmer Canyon block (PCB) and Laramie Peak block (LPB) are labeled. The black dashed line denotes the CDROM refraction line and the nearby triangles are the broadband seismometers. The Cheyenne Belt suture (CB) is the white line, dashed where inferred. Other major shear zones are denoted with gray lines: LPSZ, Laramie Peak shear zone; FLSZ, Farwell Mt.-Lester Mt. suture zone; SFSZ, Soda Creek-Fish Creek shear zone; SGSZ, Skin Gulch shear zone. The location of the Stateline Kimberlite District (SLKD) and Iron Mountain District (IMD) are shaded red. b) A structural map of southeast Wyoming from *Resor and Snoke, 2005*.

Data and Deconvolution Methodology

Our P wave receiver function dataset is constructed from 58 P wave events at 30°–100° epicentral distance with body wave magnitudes >5.6 and our S wave receiver function dataset constructed from five S wave and four SKS events from 55°–85° and >85° epicentral distances, respectively (Fig. 2). For S wave arrivals, the distance range is restricted to avoid interference with secondary arrivals (Wilson et al., 2006; Yuan et al., 2006). All events are rotated into the P-SV-SH coordinate system (Vinnik, 1977) and band-pass-filtered at 0.1–1 Hz and 0.05–0.5 Hz for the P and S wave receiver function datasets. S wave events are visually inspected and only events with SV-dominant polarization and low pre-event noise are used. For our P wave tomography model, 1600 travel-time residuals are measured from 78 teleseismic P wave events using a multi-channel cross-correlation algorithm (VanDecar and Crossen, 1990). The arrival times are inverted for P wave velocity perturbation using a standard least-squares algorithm resulting in a 74% variance reduction of the P wave residuals (S. Newton, unpublished data, M.S. thesis, 2008).

Our deconvolution scheme is based upon a new methodology that explicitly includes pure-mode scattering that arrives on the direct arrival component, i.e. P-P scattering on the P-component P wave receiver function and S-S scattering on the SV-component S wave receiver function. This technique exploits the quasi minimum-phase nature of the direct component receiver function and results in a full 3-component receiver function estimate for each event bin (Baig et al., 2005; Bostock, 2004; Mercier et al., 2006). The source spectra are estimated by fitting a smoothed spline to the observed P and SV-component spectra for each event.
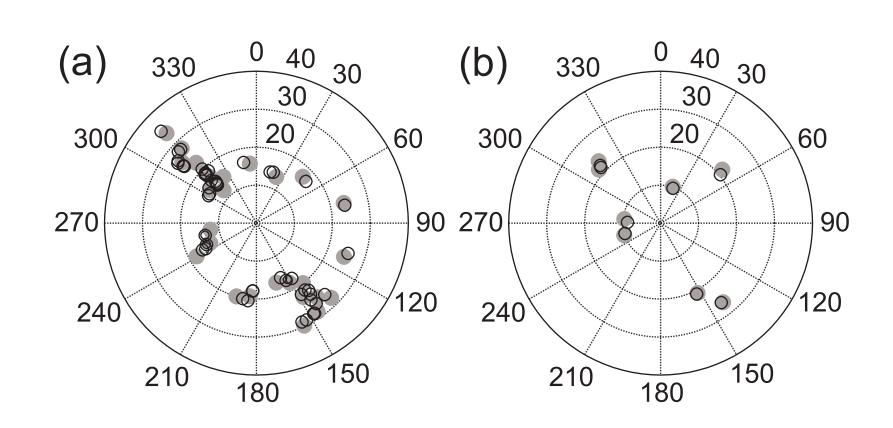

Figure 2. Polar plots of teleseismic events and event bins used in receiver function processing. Black circles denote events and gray circles denote event bins. a) P wave events. b) S wave events.

$$x(t) = s(t) * g(t) \qquad (1)$$

$$\log\{X(w)\} = \log\{S(w)\} + \log\{G(w)\} \qquad (2)$$

$$\begin{bmatrix} I_3 & 1 & \cdots & 0 \\ 0 & 1 & \ddots & \vdots \\ \vdots & \ddots & \ddots & 0 \\ I_3 & 0 & \cdots & 1 \\ 0 & 0 & \cdots & 1 \end{bmatrix} \begin{bmatrix} \log\{G(w)\} \\ \log\{S_1(w)\} \\ \vdots \\ \log\{S_M(w)\} \end{bmatrix} = \begin{bmatrix} \log\{X_1(w)\} \\ \log\{\tilde{S}_1(w)\} \\ \vdots \\ \log\{X_M(w)\} \\ \log\{\tilde{S}_M(w)\} \end{bmatrix} \qquad (3)$$

$$p \sum_{i=1}^{n} \left(\log\{X(w_i)\} - f(w_i) \right)^2 + (1-p) \int f''(w)^2 \, dw \qquad (4)$$
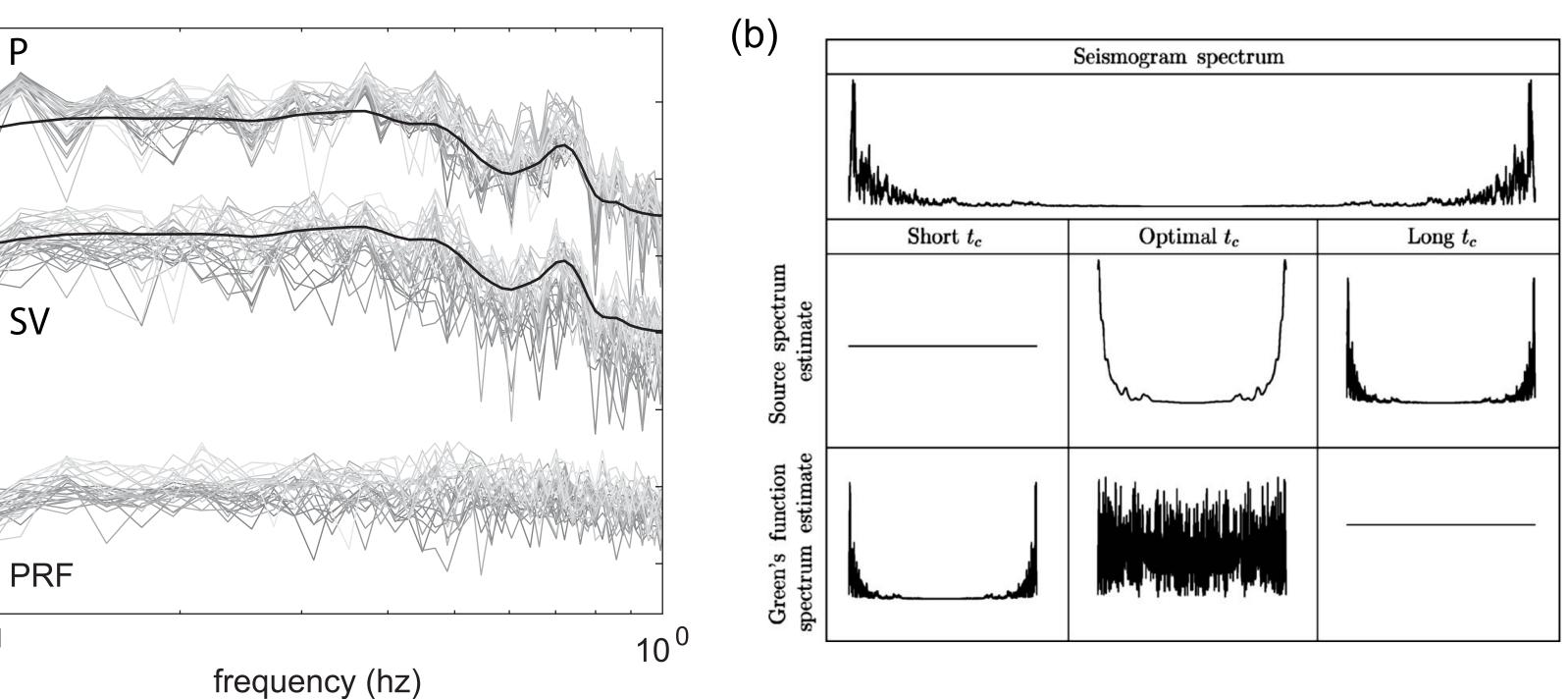

Figure 3. a) Source function estimation for a P wave event. The power spectra of the recorded seismic traces and the resulting receiver functions are labeled and plotted as gray lines. The P- and SV-component spectra are offset for clarity and labeled. The black lines denote the estimated power spectrum of the source function as a result of stacking the spline smoothed P-component spectra. The P wave receiver function spectra are the result the least-squares inversions of equation (3). b) The effect of spectral smoothing on the resulting receiver function from *Mercier et al., 2006*. The optimal smoothing results in relatively white spectrum.
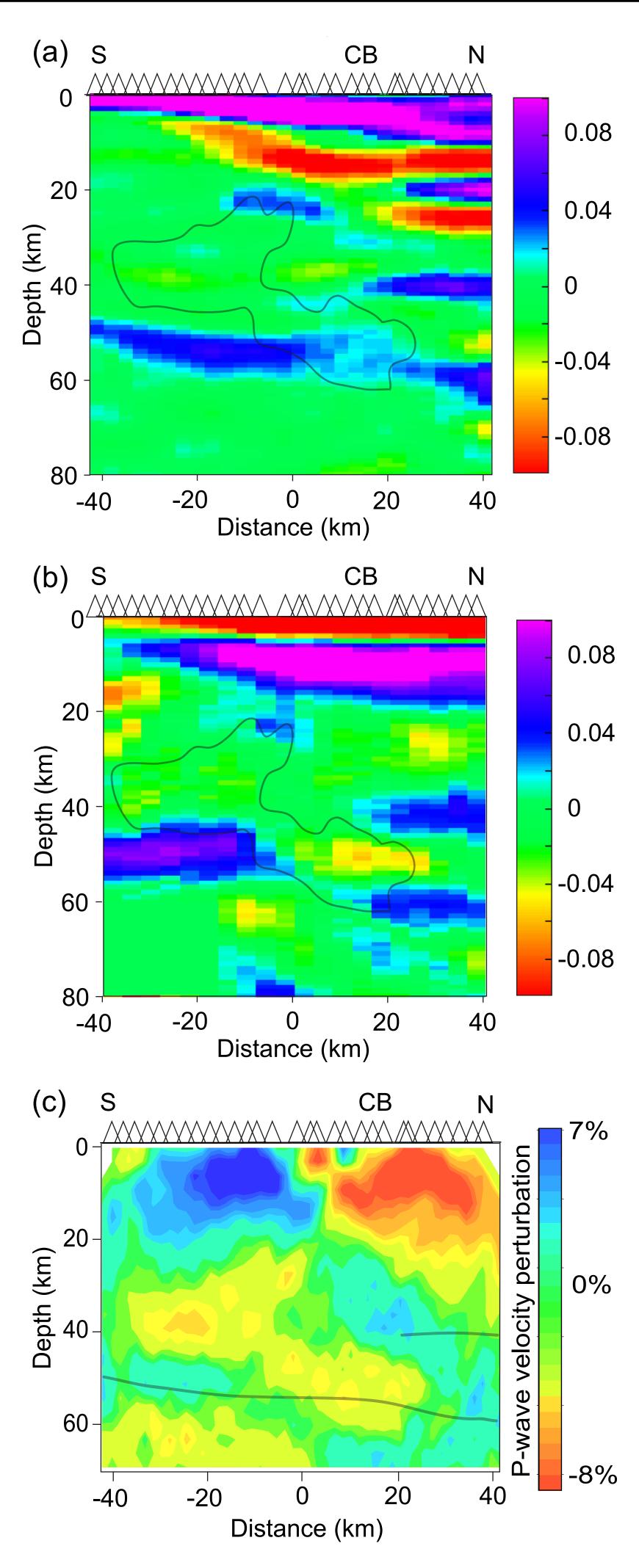

Figure 4. Laramie array results. Triangle symbols denote the station locations and the Cheyenne belt (CB) is labeled. a) P wave receiver function image. b) S wave receiver function image. c) Teleseismic P wave tomography model. The gray lines denoted the base of the Archean and Proterozoic crust interpreted from a). In b) the image is muted from 60 to 80 km depth between -20 and -40 km distance due to a lack of data in this region, e.g. see Figure 5b. Blue and red colors in (a) and (b) denote positive and negative shear velocity contrasts with respect to increasing depth. The gray line on images (a) and (b) is the -3.5% P wave velocity perturbation contour from (c).

Figure 5. Converted wave ray paths. a) Pds rays for P wave receiver function image. b) Sdp rays for S wave receiver functions. The dashed lines show the locations of the Archean and Proterozoic Moho as interpreted from the CCP images (Fig. 4b,c). The rays in (a) that appear to be near normal incidence are the projection of out of plane events (Fig. 2b).

Figure 6. Seismic amplitude modeling. (a) P wave receiver function stacks from northwest (NW) and southeast (SE) backazimuth gathers for the ten southernmost stations for 0.04–0.06 s/km ray parameter events. (b) P and S wave receiver function stacked trace with bootstrapped standard errors from the six northernmost stations. (c) P wave velocity models that explain the observed amplitudes from (b). The black line denotes the best fit model and the gray shading shows velocity models fitting the observed amplitudes within one standard error. The dashed lines show the CDROM refraction models from Snelson et al. (2005) (denoted CDROM 1) and Levander et al. (2005) (denoted CDROM 2). The black horizontal bars show the measured xenolith velocities from Leucite Hills (LHX) and the State Line diatremes (SLX) (Farmer et al., 2005).
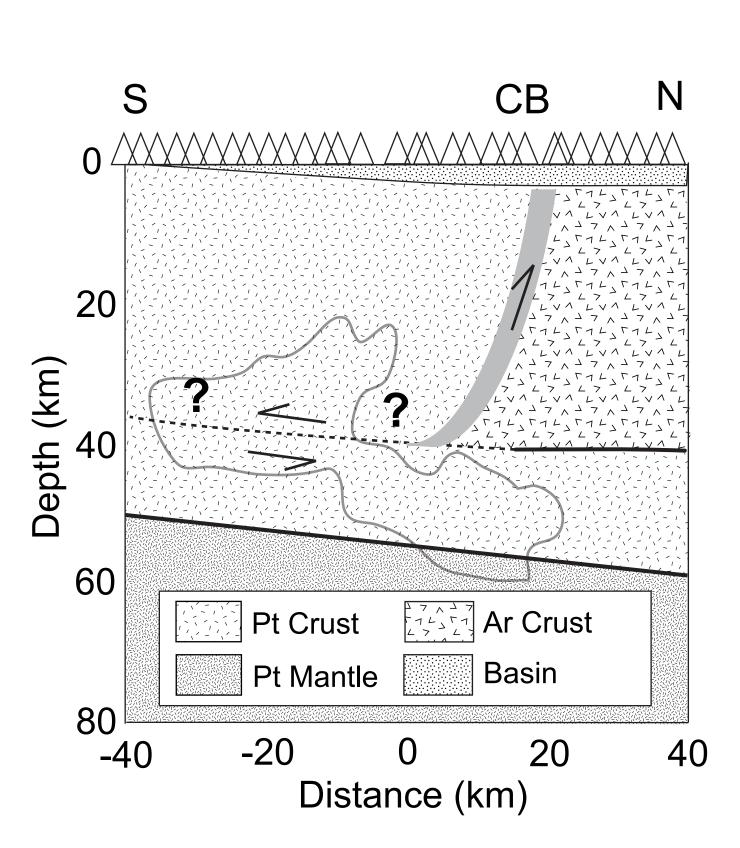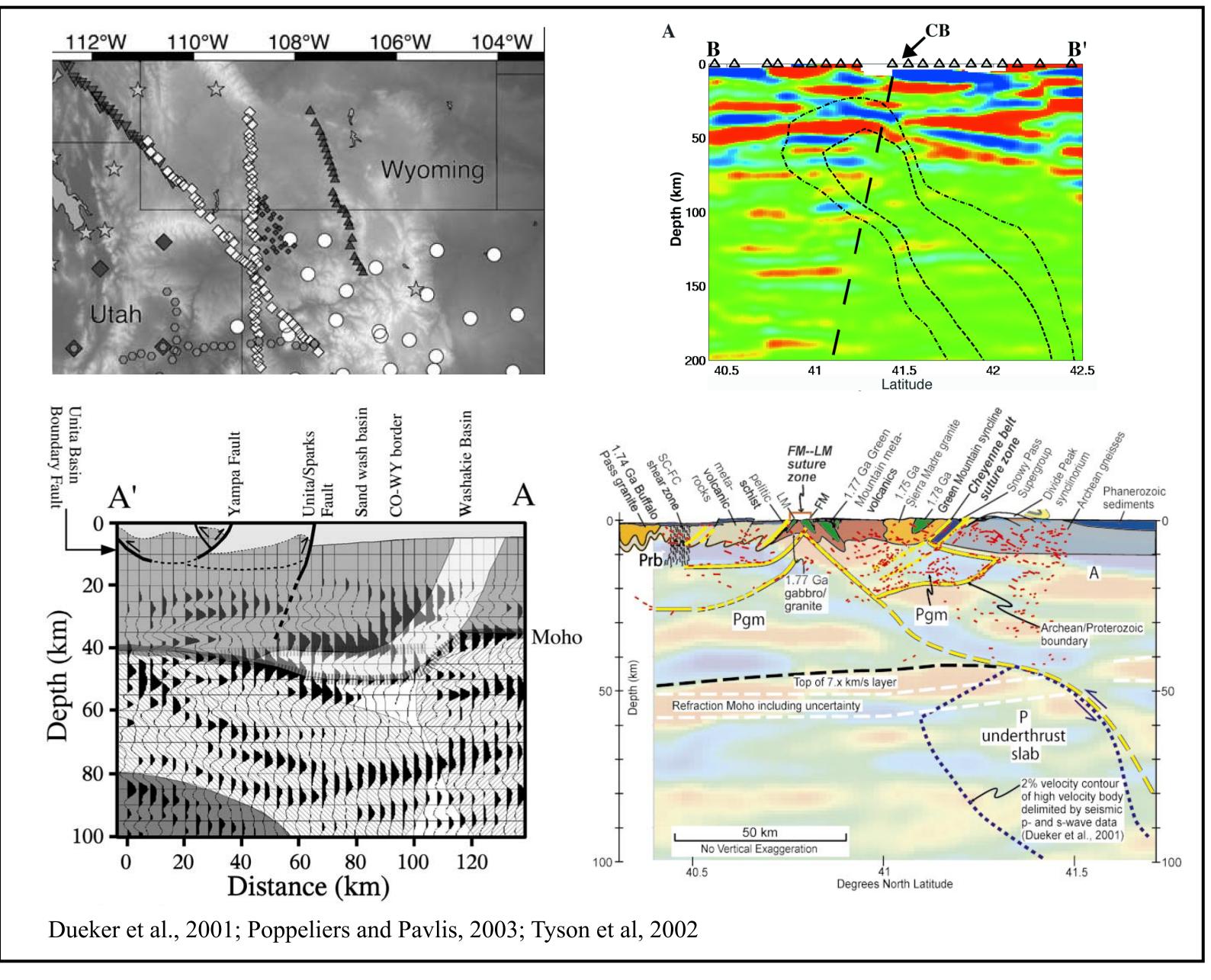
Figure 7. Geologic interpretation. The location of the Cheyenne belt (gray line) is inferred from the lateral termination of the Archean Moho observed in Figure 3. The underthrusting of the Proterozoic lower crust is accommodated by the mid crustal shear zone, denoted by the dashed black line. The sense of shearing on the Cheyenne belt and the mid crustal shear zone are denoted by arrows. The Archean Moho and Proterozoic Moho from the P wave receiver function image (Fig. 4a) are denoted by thick black lines. The gray line on the images is the -3.5% P wave velocity perturbation contour from Figure 4c.

Major Findings-

- Spectral smoothing and minimum-phase deconvolution can be used to calculate S wave receiver functions

- Seismic results show north dipping crustal structure south of the Cheyenne belt

- Both P and S wave receiver function images find a "double-Moho" north of the CB

- A north dipping Proterozoic Moho and crustal imbrication are consistent with RF amplitude modeling

- We speculate that imbrication was coeval with the uplift and deformation of the Palmer Canyon block ~1.76 Ga

- Our results are consistent with previous seismic results along the CB and suggest ubiquitous imbrication

References

Baig, A. M., M. Bostock, and J. P. Mercier (2005), Spectral reconstruction of teleseismic P Green's functions, J. Geophys. Res., 110, B08306, doi:10.1029/2005JB003625.

Bostock, M. (2004), Green's functions, source signatures, and the normalization of teleseismic wave fields, J. Geophys. Res., 109, B03303, doi:10.1029/2003JB002783.

Ken Dueker, Huaiyu Yuan, and Brian Zurek (2001), Thick-structured Proterozoic lithosphere of the Rocky Mountain region GSA Today, 11(12):4-9

Mercier, J. P., M. Bostock, and A. M. Baig (2006), Improved Green's Functions for Passive Source Structural Studies, Geophysics, 22, SI95-SI102, doi:10.1190/1.2213951.

Poppeliers, C., and G. L. Pavlis (2003), Three-dimensional, prestack, plane wave migration of teleseismic P-to-S converted phases: 2. Stacking multiple events, J. Geophys. Res., 108(B5), 2267, doi:10.1029/2001JB001583.

Tyson, A. R., S. B. Smithson, K. G. Dueker, C. T. Foster, E. A. Morozova, K. E. Karlstrom, and A. R. Chamberlain (2002), Proterozoic Farwell Mountain-Lester Mountain suture zone, northern Colorado: Subduction flip and progressive assembly of arcs, Geology, 30, 943-946.

Vinnik, L. P. (1977), Detection of waves converted from P to SV in the mantle, Physics of the Earth and Planetary Interiors, 15, 39-45.

Wilson, D. C., D. A. Angus, J. F. Ni, and S. P. Grand (2006), Constraints on the interpretation of S-to-P receiver functions, Geophys. J. Int., 165, 969-980, doi:10.1111/j.1365-246X.2006.02981.x.

Yuan, X., R. Kind, X. Li, and R. Wang (2006), The S receiver functions: synthetics and data example, Geophys. J. Int., 165, 555-564, doi:10.1111/j.1365-246X.2006.02885.x.
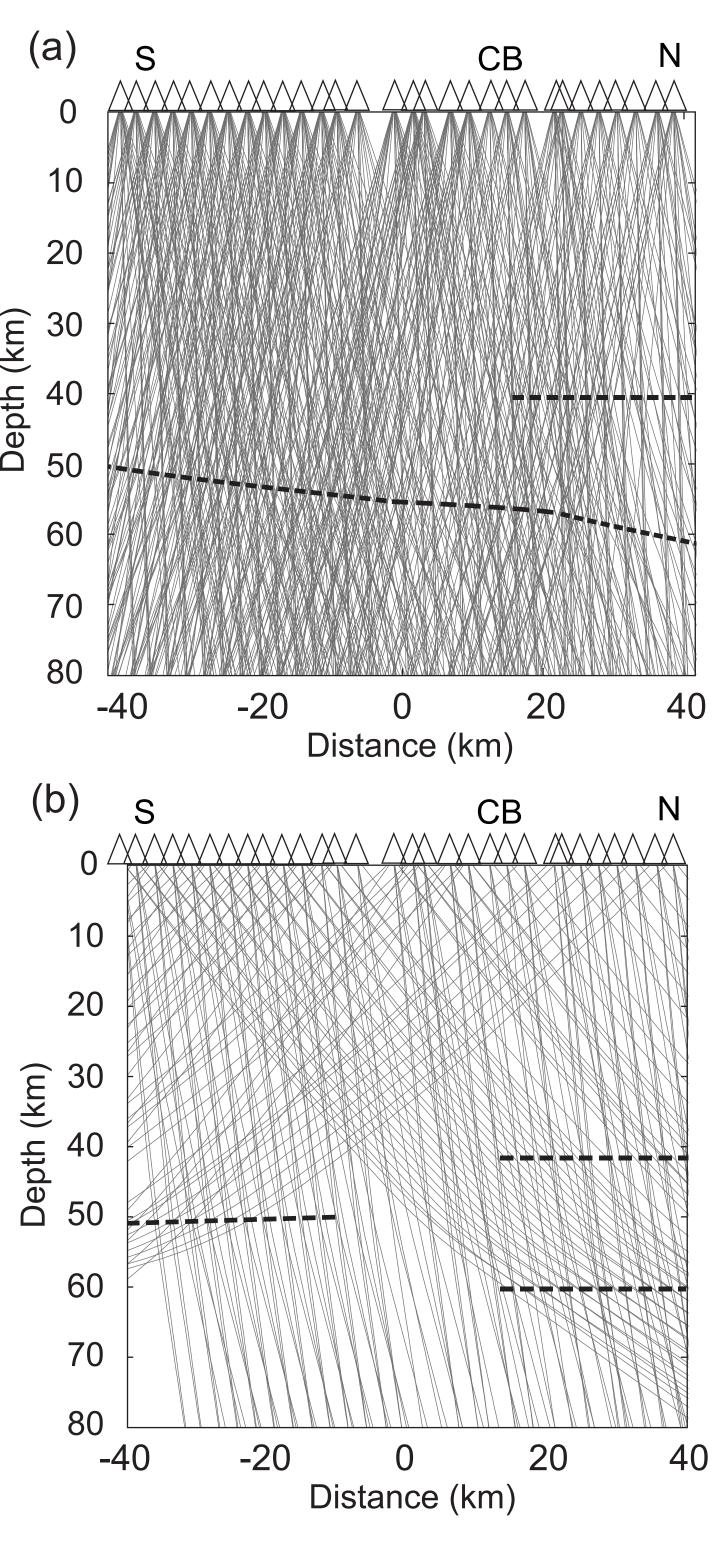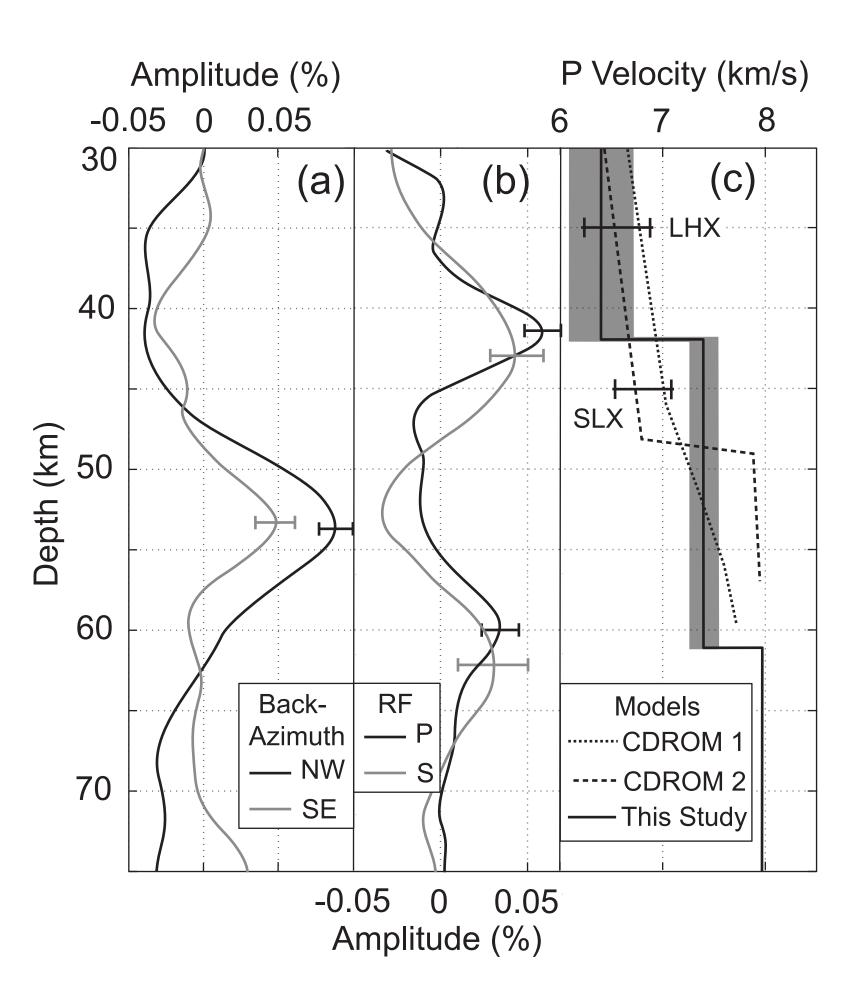
Previous Work

Dueker et al., 2001; Poppeliers and Pavlis, 2003; Tyson et al, 2002

University of Wyoming